KEK-TH-1008
KOBE-FHD-05-01
HUPD-0501

The Decay of Tau Leptons Produced in Neutrino-Nucleon Scatterings

Mayumi Aoki[1*], Kaoru Hagiwara[1,2], Kentarou Mawatari[3†], and Hiroshi Yokoya[4,5‡]

[1] *Theory Group, KEK, Tsukuba 305-0801, JAPAN*
[2] *Department of Particle and Nuclear Physics, Graduate University for Advanced Studies, Tsukuba 305-0801, JAPAN*
[3] *Graduate School of Science and Technology, Kobe University, Nada, Kobe 657-8501, JAPAN*
[4] *Department of Physics, Hiroshima University, Higashi-Hiroshima 739-8526, JAPAN*
[5] *Radiation Laboratory, RIKEN, Wako 351-0198, JAPAN*

Abstract

Energy and angular distributions of the τ decay products in the CERN-to-Gran Sasso ν_τ appearance experiments are studied for the decay modes $\tau \to \pi\nu$ and $\tau \to \ell\bar{\nu}\nu$ ($\ell = e$ or μ). We find that the decay particle distributions in the laboratory frame are significantly affected by the τ polarization. Rather strong azimuthal asymmetry of π^- and ℓ^- about the τ momentum axis is predicted, which may have observable consequences even at small statistics experiments.

*E-mail address: mayumi.aoki@kek.jp
†E-mail address: kentarou@post.kek.jp
Present address: Theory Group, KEK, Tsukuba 305-0801, JAPAN
‡E-mail address: yokoya@nt.sc.niigata-u.ac.jp
Present address: Department of Physics, Niigata University, Niigata 950-2181, JAPAN

1 Introduction

Neutrino oscillation physics is one of the most attractive field of current particle physics, and plenty of theoretical and experimental studies are revealing the amazing nature of the neutrino sector, such as their non-zero masses and the large mixings. We are now entering the stage of precise determination of the mass-squared differences including their signs and the mixing angles. The CP phase of the MNS (Maki-Nakagawa-Sakata) lepton-flavor-mixing matrix [1] also interests us.

On the other hand, it is also important to find the direct evidence of the neutrino oscillation within the three generations. It can be achieved by detecting ν_τ appearance in the long baseline neutrino oscillation experiments with the initial ν_μ beam. The CNGS (CERN Neutrino to Gran Sasso) long baseline experiments [2] with ICARUS [3] and OPERA [4] detectors aim to establish ν_τ appearance by measuring the τ lepton production events caused by the charged current (CC) interactions. They are now under construction and plan to start taking data from the year 2006. It is also expected that the CNGS experiments will improve significantly the current upper limit on θ_{13}, which is the smallest of the three mixing angles in the three-flavor MNS matrix, by measuring $\nu_\mu \to \nu_e$ transition [5]. The ν_τ CC events followed by the $\tau \to e$ decays contribute as background events to the signals of the $\nu_\mu \to \nu_e$ events. Thus, the detailed analysis of the ν_τ CC events is important in the CNGS experiments.

Since the τ lepton has the large mass, $m_\tau = 1.78$ GeV, it immediately decays into several particles always including a neutrino (ν_τ). For that reason, τ production will be detected through its decay particle distributions. On the other hand, the decay particle distributions from τ depend critically on its spin polarization. It is therefore important to consider the spin polarization of τ in addition to its production cross section.

Detailed discussions on the spin polarization of τ produced in neutrino-nucleon scattering can be found in the recent paper [6]. There, the quasi-elastic scattering (QE), the resonance production (RES) and the deep inelastic scattering (DIS) processes were considered for the τ production, and it was shown that the produced $\tau^\pm$'s have high degree of polarization, and their spin direction depends non-trivially on the energy and the scattering angle of $\tau^\pm$ in the laboratory frame.

In this article, we study the decay distributions from τ^- leptons produced via the CC interactions, especially for the CNGS experiments. We consider the τ^- production in the neutrino-nucleon scattering and its subsequent decays, for the decay modes $\tau^- \to \pi^-\nu_\tau$ and $\tau^- \to \ell^-\bar{\nu}_\ell\nu_\tau$ ($\ell = e,\, \mu$):

$$\nu_\tau + N \to \tau^- + X; \quad \tau^- \to \begin{cases} \pi^- + \nu_\tau \\ \ell^- + \bar{\nu}_\ell + \nu_\tau \end{cases} \tag{1}$$

2 Tau production

Let us start with the brief summary of the cross section and spin polarization of τ^- produced via neutrino. One can find more details in Ref. [6].

2.1 Kinematics and the formalism

We consider τ^- production by the charged current (CC) reactions off a nucleon target:

$$\nu_\tau(k) + N(p) \to \tau^-(k') + X(p'). \tag{2}$$

For the hadronic final states X, we consider three subprocesses; the quasi-elastic scattering (QE), the Δ resonance production (RES) and the deep inelastic scattering (DIS) processes. The four-momenta are parametrized in the laboratory frame as

$$\begin{aligned} k &= (E_\nu,\, 0,\, 0,\, E_\nu), \\ p &= (M,\, 0,\, 0,\, 0), \\ k' &= (E_\tau,\, p_\tau \sin\theta_\tau,\, 0,\, p_\tau \cos\theta_\tau), \end{aligned} \tag{3}$$

and the following Lorentz invariant variables are introduced

$$Q^2 = -q^2 = -(k-k')^2, \tag{4}$$

$$W^2 = (p+q)^2. \tag{5}$$

Each subprocess is distinguished by the hadronic invariant mass W: $W = M$ for QE, $M + m_\pi < W < W_{\rm cut}$ for RES. $W_{\rm cut}$ is an artificial boundary, and we regard that DIS process occurs in the regions of $W > W_{\rm cut}$[1]. We take $W_{\rm cut} = 1.4$ GeV in this report.

The differential cross section and the spin polarization vector of produced τ^- are obtained in the laboratory frame as [6]

$$\begin{aligned} \frac{d\sigma_\tau}{dE_\tau\, d\cos\theta_\tau} &= \frac{G_F^2\kappa^2}{2\pi}\frac{p_\tau}{M}\left\{\left(2W_1 + \frac{m_\tau^2}{M^2}\,W_4\right)(E_\tau - p_\tau\cos\theta_\tau) + W_2\,(E_\tau + p_\tau\cos\theta_\tau)\right. \\ &\qquad \left. + \frac{W_3}{M}\left(E_\nu E_\tau + p_\tau^2 - (E_\nu + E_\tau)p_\tau\cos\theta_\tau\right) - \frac{m_\tau^2}{M}\,W_5\right\} \\ &\equiv \frac{G_F^2\kappa^2}{2\pi}\frac{p_\tau}{M}\,F, \end{aligned} \tag{6}$$

and

$$s_x = -\frac{m_\tau \sin\theta_\tau}{2}\left(2W_1 - W_2 + \frac{E_\nu}{M}\,W_3 - \frac{m_\tau^2}{M^2}\,W_4 + \frac{E_\tau}{M}\,W_5\right)\Big/ F, \tag{7a}$$

$$s_y = 0, \tag{7b}$$

$$\begin{aligned} s_z = -\frac{1}{2}\Bigg\{&\left(2W_1 - \frac{m_\tau^2}{M^2}\,W_4\right)(p_\tau - E_\tau\cos\theta_\tau) + W_2\,(p_\tau + E_\tau\cos\theta_\tau) \\ &+ \frac{W_3}{M}\left((E_\nu + E_\tau)p_\tau - (E_\nu E_\tau + p_\tau^2)\cos\theta_\tau\right) - \frac{m_\tau^2}{M}\,W_5\cos\theta_\tau\Bigg\}\Big/ F, \end{aligned} \tag{7c}$$

where G_F is the Fermi constant and $\kappa = M_W^2/(Q^2 + M_W^2)$. $\vec{s} = (s_x, s_y, s_z)$ is defined in the τ rest frame in which the z-axis is taken along its momentum direction and the y-axis is along $\vec{k}\times\vec{k'}$, the normal of the scattering plane, in the laboratory frame. It is normalized

[1] More detailed studies on τ productions via the CC reactions have recently been reported in Ref. [7].

as $|\vec{s}| = 1/2$ for pure spin eigenstates. $W_{i=1,\ldots,5}$ are structure functions defined with the generic decomposition of the hadronic tensor,

$$W_{\mu\nu}(p,q) = -g_{\mu\nu}W_1(p\cdot q,\, Q^2) + \frac{p_\mu p_\nu}{M^2}\,W_2(p\cdot q,\, Q^2) - i\epsilon_{\mu\nu\alpha\beta}\frac{p^\alpha q^\beta}{2M^2}\,W_3(p\cdot q,\, Q^2) + \frac{q_\mu q_\nu}{M^2}\,W_4(p\cdot q,\, Q^2) + \frac{p_\mu q_\nu + q_\mu p_\nu}{2M^2}\,W_5(p\cdot q,\, Q^2), \quad (8)$$

where the totally anti-symmetric tensor $\epsilon_{\mu\nu\alpha\beta}$ is defined as $\epsilon_{0123} = 1$. These functions can be estimated for each process, QE, RES, and DIS, as follows.

2.2 Hadronic tensor

2.2.1 Quasi-elastic scattering (QE)

The hadronic tensor for the QE process, $\nu_\tau + n \to \tau^- + p$, is written by using the hadronic weak transition current J_μ as follows [8]:

$$W^{\rm QE}_{\mu\nu} = \frac{\cos^2\theta_c}{4}\sum_{\rm spins} J_\mu J_\nu{}^*\,\delta(W^2 - M^2), \quad (9)$$

where θ_c is the Cabibbo angle. J_μ is defined as

$$J_\mu \equiv \langle p(p')|\hat{J}_\mu|n(p)\rangle = \bar{u}_p(p')\,\Gamma_\mu\,u_n(p), \quad (10)$$

where Γ_μ is written in terms of the six weak form factors of the nucleon, $F^V_{1,2,3}$, F_A, F^A_3 and F_p, as

$$\Gamma_\mu = \gamma_\mu F^V_1 + \frac{i\sigma_{\mu\alpha}q^\alpha\xi}{2M}F^V_2 + \frac{q_\mu}{M}F^V_3 + \left[\gamma_\mu F_A + \frac{(p+p')_\mu}{M}F^A_3 + \frac{q_\mu}{M}F_p\right]\gamma_5. \quad (11)$$

We can drop F^V_3 and F^A_3 because of the time reversal invariance and the isospin symmetry. Moreover, the vector form factors F^V_1 and F^V_2 are related to the electromagnetic form factors of nucleons under the conserved vector current (CVC) hypothesis:

$$F^V_1(q^2) = \frac{G^V_E - \frac{q^2}{4M^2}G^V_M}{1-\frac{q^2}{4M^2}}, \quad \xi F^V_2(q^2) = \frac{G^V_M - G^V_E}{1-\frac{q^2}{4M^2}}, \quad (12)$$

where

$$G^V_E(q^2) = \frac{G^V_M(q^2)}{1+\xi} = \frac{1}{(1-q^2/M_V^2)^2} \quad (13)$$

with a vector mass $M_V = 0.84$ GeV and $\xi = 3.706$. For the axial-vector form factor F_A and the pseudoscalar form factor F_p, we use

$$F_A(q^2) = \frac{F_A(0)}{(1-q^2/M_A^2)^2}, \quad F_p(q^2) = \frac{2M^2}{m_\pi^2 - q^2}F_A(q^2), \quad (14)$$

with $F_A(0) = -1.27$ [9] and an axial-vector mass $M_A = 1.026$ GeV [10]. Notice that the pseudoscalar form factor F_p plays an important role for the polarization of τ produced by neutrino because its contribution is proportional to the lepton mass and it has the spin-flip nature, although it is not known well experimentally; see Ref. [11] for details.

2.2.2 Resonance production (RES)

The hadronic tensor for the Δ resonance production (RES) process, $\nu_\tau + n\ (p) \to \tau^- + \Delta^+\ (\Delta^{++})$, is calculated in terms of the N-Δ weak transition current J_μ as follows [8, 12, 13]:

$$W_{\mu\nu}^{\rm RES} = \frac{\cos^2\theta_c}{4} \sum_{\rm spins} J_\mu J_\nu^* \left| \frac{\sqrt{W\Gamma(W)/\pi}}{W^2 - M_\Delta^2 + iW\Gamma(W)} \right|^2 \tag{15}$$

with the running width

$$\Gamma(W) = \Gamma(M_\Delta)\, \frac{M_\Delta}{W}\, \frac{\lambda^{\frac{1}{2}}(W^2, M^2, m_\pi^2)}{\lambda^{\frac{1}{2}}(M_\Delta^2, M^2, m_\pi^2)}. \tag{16}$$

$\Gamma(M_\Delta) = 0.12$ GeV and $\lambda(a,b,c) = a^2 + b^2 + c^2 - 2(ab + bc + ca)$. The current J_μ for the process $\nu_\tau + n \to \tau^- + \Delta^+$ is parametrized as

$$J_\mu \equiv \langle \Delta^+(p')|\hat{J}_\mu|n(p)\rangle = \bar{\psi}^\alpha(p')\, \Gamma_{\mu\alpha}\, u_n(p), \tag{17}$$

where ψ^α is the spin-3/2 particle wave function and the vertex $\Gamma_{\mu\alpha}$ is expressed in terms of the eight weak form factors $C_{i=3,4,5,6}^{V,A}$ as

$$\begin{aligned}\Gamma_{\mu\alpha} = &\left[\frac{g_{\mu\alpha}\, \not{q} - \gamma_\mu q_\alpha}{M} C_3^V + \frac{g_{\mu\alpha}\, p'\cdot q - p'_\mu q_\alpha}{M^2} C_4^V + \frac{g_{\mu\alpha}\, p\cdot q - p_\mu q_\alpha}{M^2} C_5^V + \frac{q_\mu q_\alpha}{M^2} C_6^V \right] \gamma_5 \\ &+ \frac{g_{\mu\alpha}\, \not{q} - \gamma_\mu q_\alpha}{M} C_3^A + \frac{g_{\mu\alpha}\, p'\cdot q - p'_\mu q_\alpha}{M^2} C_4^A + g_{\mu\alpha} C_5^A + \frac{q_\mu q_\alpha}{M^2} C_6^A. \end{aligned} \tag{18}$$

By using the isospin invariance and the Wigner-Eckart theorem, we obtain another N-Δ weak transition current as $\langle \Delta^{++}|\hat{J}_\mu|p\rangle = \sqrt{3}\langle \Delta^+|\hat{J}_\mu|n\rangle$. From the CVC hypothesis, $C_6^V = 0$ and the other vector form factors $C_{i=3,4,5}^V$ are related to the electromagnetic form factors. Assuming the magnetic dipole dominance [14], we have $C_5^V = 0$ and $C_4^V = -\frac{M}{M_\Delta}\, C_3^V$. For C_3^V, we adopt the modified dipole parameterizations [15, 16]:

$$C_3^V(q^2) = \frac{C_3^V(0)}{\left(1 - \frac{q^2}{M_V^2}\right)^2} \frac{1}{1 - \frac{q^2}{4M_V^2}} \tag{19}$$

with $C_3^V(0) = 2.05$ and $M_V = 0.735$ GeV. For the axial form factors, we use [15]

$$C_5^A(q^2) = \frac{C_5^A(0)}{(1 - \frac{q^2}{M_A^2})^2} \frac{1}{1 - \frac{q^2}{3M_A^2}}, \quad C_6^A(q^2) = \frac{M^2}{m_\pi^2 - q^2} C_5^A(q^2), \tag{20}$$

with $C_5^A(0) = 1.2$ and $M_A = 1.0$ GeV. For C_3^A and C_4^A, $C_3^A = 0$ and $C_4^A = -\frac{1}{4} C_5^A$ give good agreements with the data [12]. As in the case of $F_p(q^2)$ in the QE process, the pseudoscalar form factor $C_6^A(q^2)$ has significant effects on the τ production cross section and the τ polarization [11].

2.2.3 Deep inelastic scattering (DIS)

In the DIS region, the hadronic tensor is estimated by using the quark-parton model:

$$W_{\mu\nu}^{\rm DIS}(p,q) = \sum_{q,\bar{q}} \int \frac{d\xi}{\xi} f_{q,\bar{q}}(\xi, Q^2) K_{\mu\nu}^{(q,\bar{q})}(p_q, q), \tag{21}$$

where $p_q = \xi p$ is the four-momentum of the scattering quark, ξ is its momentum fraction, and $f_{q,\bar{q}}$ are parton distribution functions (PDFs) inside a nucleon. The quark tensor $K_{\mu\nu}^{(q,\bar{q})}$ is

$$\begin{aligned} K_{\mu\nu}^{(q,\bar{q})}(p_q, q) =& \delta(2\, p_q \cdot q - Q^2 - m_{q'}^2) \\ & \times 2[-g_{\mu\nu}(p_q \cdot q) + 2p_{q\mu}p_{q\nu} + p_{q\mu}q_\nu + q_\mu p_{q\nu} \mp i\epsilon_{\mu\nu\alpha\beta}p_q^\alpha q^\beta]. \end{aligned} \tag{22}$$

The upper sign should be taken for quarks and the lower sign for antiquarks. We retain the final quark mass $m_{q'}$ for the charm quark as $m_c = 1.25$ GeV, but otherwise we set $m_{q'} = 0$. In the calculation, we used MRST2002 [17] for the PDFs[2].

By neglecting both the nucleon mass and the initial quark masses, the following relations are obtained:

$$W_1(p\cdot q, Q^2) = F_1(\xi, Q^2), \quad W_{i=2,\ldots,5}(p\cdot q, Q^2) = \frac{M^2}{p\cdot q}\, F_{i=2,\ldots,5}(\xi, Q^2). \tag{23}$$

Here,

$$\begin{aligned} F_1 = \sum_{q,\bar{q}} f_{q,\bar{q}}(\xi, Q^2), \quad F_2 = 2\sum_{q,\bar{q}} \xi\, f_{q,\bar{q}}(\xi, Q^2), \\ F_3 = 2\sum_{q} f_q(\xi, Q^2) - 2\sum_{\bar{q}} f_{\bar{q}}(\xi, Q^2), \quad F_4 = 0, \quad F_5 = 2\sum_{q,\bar{q}} f_{q,\bar{q}}(\xi, Q^2), \end{aligned} \tag{24}$$

where $\xi = Q^2/2p\cdot q \equiv x$ for massless final quarks ($m_{q'} = 0$), and $\xi = x/\lambda$ with $\lambda = Q^2/(Q^2 + m_{q'}^2)$ for $q' = c$. In fact, the differential cross section, Eq. (6), does not satisfy the positivity condition near the threshold with this naive replacement. We modify the W_1 structure function as $W_1 = (1 + \frac{\xi M^2}{p\cdot q})F_1$ in order to preserve the positivity [6].

2.3 Polarization of produced τ^- at a fixed neutrino energy

We summarize the cross section and spin polarization of τ^- produced in neutrino-nucleon scattering for isoscalar targets at the incident neutrino energy $E_\nu = 10$ GeV on the $p_\tau\cos\theta_\tau$-$p_\tau\sin\theta_\tau$ plane, where p_τ and θ_τ are the τ momentum and the scattering angle in the laboratory frame.

In Fig. 1, the differential cross sections $d\sigma/dp_z\, dp_T$, obtained from Eq. (6), are shown as a contour map[3], where $p_z = p_\tau\cos\theta_\tau$ and $p_T = p_\tau\sin\theta_\tau$. Only the contours of the DIS cross section are plotted to avoid too much complexity. Each contour gives the value of

[2]We adopt a naive extrapolation of the parton model calculation for low Q^2 in the $W > W_{\rm cut}$ region, by freezing the PDFs when $Q^2 < Q_0^2$ (=1.25 GeV^2).

[3]It must be noted that this contour map differs from Fig. 11 of Ref. [6], where $d\sigma/dE_\tau\, d\cos\theta_\tau$ is plotted.

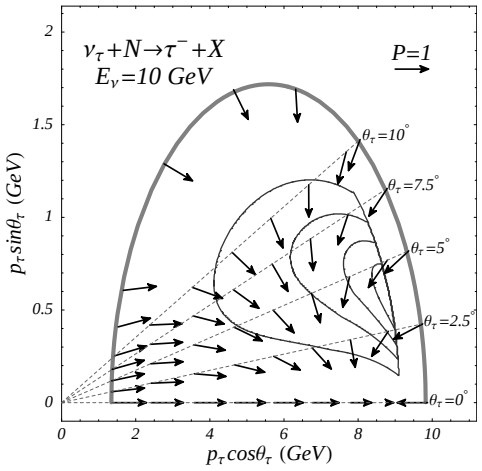

Fig. 1: The contour map of the DIS cross section on the $p_\tau \cos\theta_\tau$-$p_\tau \sin\theta_\tau$ plane for the $\nu_\tau N \to \tau^- X$ process at $E_\nu = 10$ GeV in the laboratory frame. The kinematical boundary is shown by the thick curve. The QE process contributes along the boundary, and the RES process contributes just inside of the boundary. The τ polarization are shown by the arrows. The length of the arrows give the degree of polarization, and the direction of arrows give that of the τ spin in the τ rest frame. The size of the 100% polarization ($P = 1$) arrow is shown as a reference. The arrows are shown along the laboratory scattering angles, $\theta_\tau = 0°$, 2.5°, 5°, 7.5°, and 10°, as well as along the kinematical boundary.

the differential cross section in the unit of fb/GeV^2; the outermost line is 1 fb/GeV^2 and the innermost line is for 4 fb/GeV^2. The kinematical boundary is shown by the thick curve. The QE process contributes along the boundary, and the RES process contributes just inside of the boundary. The contour map shows that the contributions in the forward scattering angles in the larger p_τ side are important. In that region, the cross sections of QE and RES are also large and comparable to that of DIS.

The polarization vector $\vec{s}$, Eq. (7), of τ^- is also shown in Fig. 1. The length of each arrow gives the degree of polarization ($0 \le P = 2|\vec{s}| \le 1$) at each kinematical point and its orientation gives the spin direction in the τ rest frame. The produced τ^- have high degree of polarization, but their spin directions significantly deviate from the massless limit predictions, where all τ^- should be purely left-handed. Since s_x of Eq. (7) turns out to be always negative, the spin vector points to the direction of the initial neutrino momentum axis. Qualitative feature of the results can be understood by considering the helicity amplitudes in the center of mass (CM) frame of the scattering particles and the effects of Lorentz boost from the CM frame to the laboratory frame. For instance, when we consider the neutrino-quark scattering in their CM frame, produced τ^- has fully left-handed polarization at all scattering angle due to the $V-A$ interactions and the angular momentum conservation. After the Lorentz boost, higher energy τ's in the laboratory frame preserve the left-handed polarization since those τ's have forward scattering angles also in the CM frame. On the other hand, lower energy τ's in the laboratory frame tend to have right-handed polarization since they are produced in the backward direction in the CM frame. Also note that $s_x < 0$ holds always because the polarization vector points to the collision point in the CM frame. See more details in Ref. [6]. Let us stress that

these features of the polarization of τ^- play an important role in the following analysis.

2.4 Polarization of produced τ^- in the CNGS experiments

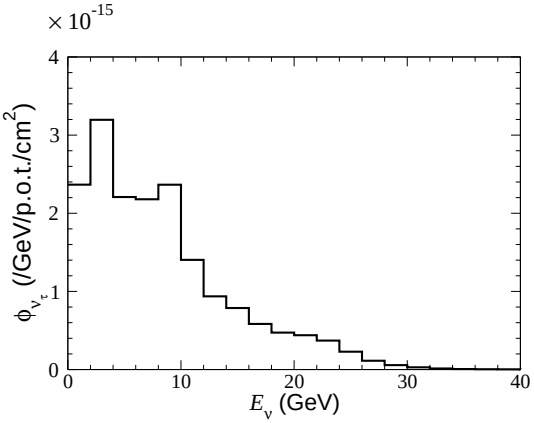

Fig. 2: The incoming ν_τ flux with the three-neutrino model in the CNGS experiments. The neutrino oscillation probabilities are calculated for a set of parameters: $\delta m^2_{12} = 8.2 \times 10^{-5}\,\mathrm{eV}^2$ and $\delta m^2_{13} = 2.5 \times 10^{-3}\,\mathrm{eV}^2$, $\sin^2 2\theta_{12,\,23,\,13} = 0.8$, 1, 0, respectively, the CP phase $\delta_{\mathrm{MNS}} = 0^\circ$, and the matter density $\rho = 3$ g/cm^3.

In the CNGS experiments, ν_μ beam is produced at CERN-PS, which is expected to deliver 4.5×10^{19} protons on target (p.o.t.) per year. The beam is optimized for ν_τ appearance with a mean neutrino energy of about 17 GeV. Fig. 2 shows the expected ν_τ flux

$$\phi_{\nu_\tau}(E_\nu) = \sum_{\ell=e,\,\mu} \phi_{\nu_\ell}(E_\nu) \times P_{\nu_\ell \to \nu_\tau}(E_\nu) \tag{25}$$

at Gran Sasso with the baseline length of $L = 732$ km from CERN. Here $\phi_{\nu_\ell}(E_\nu)$ are the initial ν_ℓ fluxes ($\ell = e,\,\mu$) [2] and $P_{\nu_\ell \to \nu_\tau}(E_\nu)$ are the $\nu_\ell \to \nu_\tau$ oscillation probabilities in the three-neutrino model. The fraction ν_e/ν_μ in the initial fluxes is less than 1%. The neutrino oscillation probabilities are calculated for a set of the three neutrino model parameters: two mass-squared differences $\delta m^2_{12,\,13}$, three mixing angles $\theta_{12,\,23,\,13}$ and the CP phase δ_{MNS} in the MNS matrix [1], and the matter density ρ. The CHOOZ [18] and Palo Verde [19] reactor experiments give the upper bounds on $\sin^2 2\theta_{13}$, as $\sin^2 2\theta_{13} < 0.16$ for $\delta m^2_{13} = 2.5 \times 10^{-3}\,\mathrm{eV}^2$. The values of δm^2_{12} and $\sin^2 2\theta_{12}$ are constrained by the observations of the solar neutrinos [20] and the KamLAND experiment [21], and these of δm^2_{13} and $\sin^2 2\theta_{23}$ by the atmospheric neutrino observation at Super-Kamiokande [22] and the K2K experiment [23]. No constraint on the CP phase has been given by the present neutrino experiments. In our analysis, we take the following values for the neutrino oscillation parameters:

$$\begin{gathered} \delta m^2_{12} = 8.2 \times 10^{-5}\,\mathrm{eV}^2, \quad \delta m^2_{13} = 2.5 \times 10^{-3}\,\mathrm{eV}^2, \\ \sin^2 2\theta_{12} = 0.8, \quad \sin^2 2\theta_{23} = 1, \quad \sin^2 2\theta_{13} = 0, \quad \delta_{\mathrm{MNS}} = 0^\circ, \end{gathered} \tag{26}$$

with the constant matter density of $\rho = 3$ g/cm^3. Here we assume the so-called normal hierarchy. Because of setting $\sin^2 2\theta_{13} = 0$, the neutrino oscillation probabilities are

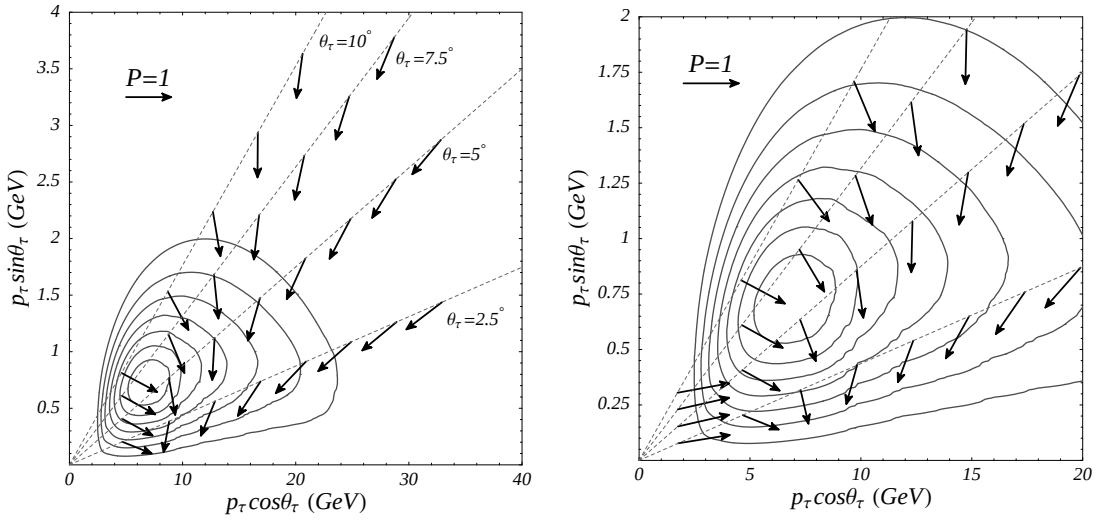

Fig. 3: The contour map of the number of τ^- production events on the $p_\tau \cos\theta_\tau$-$p_\tau \sin\theta_\tau$ plane in the CNGS experiments. The τ^- polarization are shown by the arrows. The length of the arrows give the degree of polarization, and the direction of arrows give that of the τ^- spin in the τ^- rest frame. The size of the 100% polarization ($P = 1$) arrow is shown as a reference. The arrows are shown along the laboratory scattering angles, $\theta_\tau = 2.5°$, 5°, 7.5°, and 10°. The right figure is an enlargement of the left figure.

approximately described by those in the two neutrino (ν_μ and ν_τ) model. See e.g., Ref. [24] for details.

Taking into account the CNGS neutrino flux shown in Fig. 2, we show the distributions of events and polarization vectors of τ^- on the $p_\tau \cos\theta_\tau$-$p_\tau \sin\theta_\tau$ plane in Fig. 3. The right figure is an enlargement of the left figure to show the polarization vectors in detail for the important region of large cross section. The initial neutrino energy is integrated out with the incoming ν_τ flux, $\phi_{\nu_\tau}(E_\nu)$ of Eq. (25), whereas it is fixed at 10 GeV in Fig. 1. The number of τ^- production events for all the QE, RES and DIS processes are included in the contour map, where we assume 5 years with 4.5×10^{19} p.o.t./year of the primary proton beam and the 1.65 kton size detector, which are the current plan of the OPERA experiment [4]. Each contour gives a number of events per GeV^2; the outermost line corresponds to 1 event/GeV^2, and the innermost line is for 7 events/GeV^2. The contour map shows that there are many events around E_τ=10 GeV, and around $\theta_\tau = 5°$. As for the polarization vectors, the dependence on the energy and the scattering angle of τ^- is rather smooth as compared to that in Fig. 1 because of the integration of the incident neutrino energy. As the right figure shows, however, the direction of the τ polarization is still non-trivial in the region which has many events.

3 Tau decay

3.1 Tau decay in the τ rest frame

Before turning to the τ decay in the CNGS experiments, we give the formulas of the energy and angular distributions of the decay particles, especially π^- and ℓ^-, from the

polarized τ^- lepton in the τ rest frame. The decay distributions in the laboratory frame can be easily obtained by simple Lorentz transformation. Here again we note that the z-axis of the rest frame, in which we calculate the spin polarization vector of τ, is taken along its momentum direction in the laboratory frame.

The decay distribution of π^- via the decay mode $\tau^- \to \pi^-\nu_\tau$ is given as

$$\frac{1}{\Gamma_\tau}\frac{d\Gamma_\pi}{d\hat{E}_\pi d\hat{\Omega}_\pi} = B_\pi \frac{1}{4\pi}\left(1 + \frac{2\hat{\vec{s}}\cdot\hat{\vec{p}}_\pi}{\hat{p}_\pi}\right)\delta(\hat{E}_\pi - (m_\tau^2+m_\pi^2)/2m_\tau), \tag{27}$$

where Γ_τ is the total decay width of τ and $B_\pi = B(\tau \to \pi\nu) = 11.06\%$ [9] is the decay branching fraction. All the frame dependent variables with hat ($\hat{}$) symbols are those in the τ rest frame. The energy of π is fixed as $\hat{E}_\pi = (m_\tau^2 + m_\pi^2)/2m_\tau$, because of the 2-body decay kinematics. The angular distribution of π^- is dictated by the τ^- polarization, and π^- prefers to be emitted along the τ polarization direction.

Similarly, the decay distribution of ℓ^- via the decay mode $\tau^- \to \ell^-\bar{\nu}_\ell\nu_\tau$ ($\ell = e, \mu$) is given as

$$\begin{aligned}\frac{1}{\Gamma_\tau}\frac{d\Gamma_\ell}{d\hat{E}_\ell d\hat{\Omega}_\ell} = B_\ell \frac{1}{4\pi}&\frac{2}{\hat{E}_{\rm max}^4 f(m_\ell^2/m_\tau^2)} \\ &\times \hat{p}_\ell\hat{E}_\ell\left[3\hat{E}_{\rm max} - 2\hat{E}_\ell - \frac{m_\ell^2}{\hat{E}_\ell} + \frac{2\hat{\vec{s}}\cdot\hat{\vec{p}}_\ell}{\hat{p}_\ell}\frac{\hat{p}_\ell}{\hat{E}_\ell}\left(\hat{E}_{\rm max} - 2\hat{E}_\ell + \frac{m_\ell^2}{m_\tau}\right)\right],\end{aligned} \tag{28}$$

where $\hat{E}_{\rm max} = (m_\tau^2 + m_\ell^2)/2m_\tau$ and the branching fraction of $\tau \to \ell\bar{\nu}\nu$, B_ℓ, is 17.84% for $\ell = e$ and 17.37% for $\ell = \mu$ [9]. The normalization function is $f(y) = (1 - 8y + 8y^3 - y^4 - 12y^2\ln y)/(1+y)^4$. The distribution of ℓ^- depends on its energy, and has a peak in the high energy. Furthermore, the high energy ℓ^- tends to be emitted against the direction of the τ spin, although the impact is smaller than that of the π case. It is meaningful to notice that, therefore, π^- and ℓ^- tend to have the opposite preference of the τ spin dependence on their angular distribution.

3.2 Tau decay in the CNGS experiments

In this section, we present our results of the decay particle distributions from τ^- leptons produced by the CC interactions for the CNGS experiments. Main feature of our analysis is to deal with the proper spin polarization of τ^- which is calculated for each production phase space, shown in Fig. 3. In order to show the effects of the τ polarization on the decay distributions, we compare the results with unpolarized τ decays and also with completely left-handed τ decays.

The events of the decay distributions for i = π, ℓ are given by

$$\begin{aligned}\frac{dN_{\rm i}}{dE_{\rm i}d\Omega_{\rm i}} =& A\int_{E_\nu^{\rm thr}}^{E_\nu^{\rm max}} dE_\nu\,\phi_{\nu_\tau}(E_\nu)\int_{c_{\rm min}}^{1} d\cos\theta_\tau\int_{E_-}^{E_+} dE_\tau \frac{d\sigma_\tau}{dE_\tau d\cos\theta_\tau}(E_\nu) \\ &\times \frac{1}{\Gamma_\tau}\frac{d\Gamma_{\rm i}}{dE_{\rm i}d\Omega_{\rm i}}\left(E_\tau, \theta_\tau, \vec{s}(E_\nu, E_\tau, \theta_\tau)\right),\end{aligned} \tag{29}$$

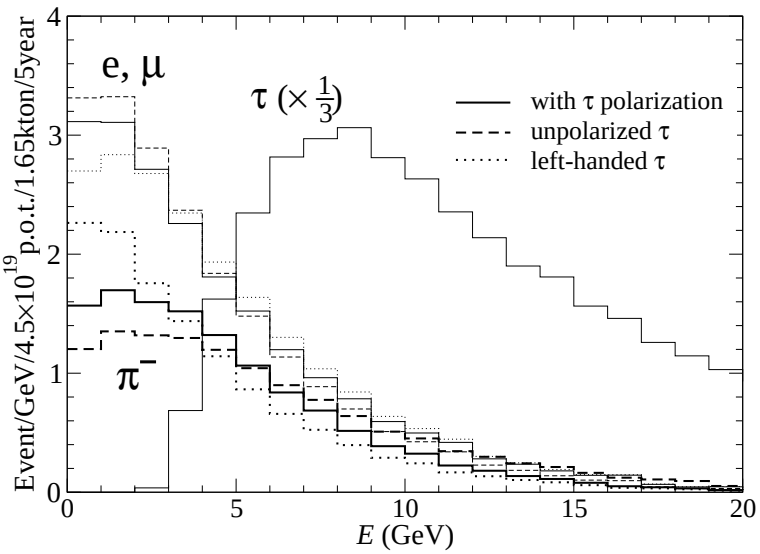

Fig. 4: Energy distributions of π^- (thick lines) and $\ell^-(=e^-,\,\mu^-)$ (medium-thick lines) in the decay of τ^- produced in the neutrino-nucleon CC interactions for the CNGS experiments. 5 years running with 4.5×10^{19} p.o.t./year of the primary proton beam and 1.65 kton detector are assumed. Solid, dashed, and dotted lines shows the energy distributions with the predicted τ polarization, unpolarized, and purely left-handed cases, respectively. The estimated number of τ^- production is also shown by a thin solid line with respect to the τ energy (E_τ).

where A is the number of active targets, $E_\nu^{\rm max}$ is the maximum value of neutrino energy in the flux, $E_\nu^{\rm thr}=m_\tau+m_\tau^2/2M$ is the threshold energy to produce τ lepton off a nucleon, and the other integral ranges are given by

$$\begin{aligned}
{\rm c}_{\rm min}(E_\nu) &= \sqrt{1+M/E_\nu+M^2/E_\nu^2-m_\tau^2/4E_\nu^2-M^2/m_\tau^2},\\
E_\pm(E_\nu,\theta_\tau) &= (b\pm\sqrt{b^2-ac})/a,
\end{aligned}$$

where $a=(E_\nu+M)^2-E_\nu^2\cos^2\theta_\tau$, $b=(E_\nu+M)(ME_\nu+m_\tau^2/2)$, $c=m_\tau^2E_\nu^2\cos^2\theta_\tau+(ME_\nu+m_\tau^2/2)^2$. Here, all the frame dependent variables are defined in the laboratory frame. E_τ and θ_τ dependence of $d\Gamma_{\rm i}/dE_{\rm i}d\Omega_{\rm i}$ appear by the Lorentz transformation from the τ rest frame to the laboratory frame. Although we retain only the π or ℓ momenta in the above formula, more exclusive measurements may be possible. For example, a well-developed emulsion detector used in OPERA experiment [4] can detect the kink of τ decay and can measure the scattering angle of τ with the accuracy of mrad, and also the τ flight length is measurable. Therefore it would be possible to do more detailed analysis of τ events, if there were enough statistics.

Fig. 4 shows the energy distributions of π^- (thick lines) and $\ell^-(=e^-,\,\mu^-)$ (medium-thick lines) decayed from τ^- produced in the neutrino-nucleon CC interactions. We assume the same configuration of the experimental setup as Fig. 3, i.e., 5 years running with 4.5×10^{19} p.o.t. per year of the primary proton beam and 1.65 kton size detector for the OPERA experiment [4]. (For the ICARUS experiment, 2.35 kton of liquid Argon detector mass and 10 years running are planned [3], so that more statistics are expected.) For each decay mode, solid lines show the distributions from the decay of τ^- with the

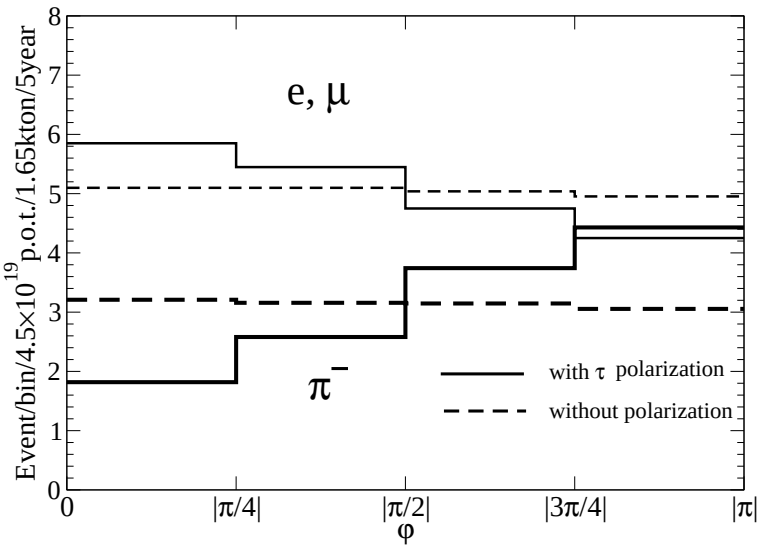

Fig. 5: Azimuthal angle distribution of π^- (thick lines) and ℓ^- (thin lines). The setup configurations, such as neutrino flux, detector size etc., are the same as Fig. 4. Solid lines show the distributions from τ^- with the predicted τ polarization, and dashed lines show those with the unpolarized τ case. The results of purely left-handed τ are the same as those for the unpolarized τ.

predicted τ polarization. For comparison, dashed and dotted lines show those of unpolarized τ and purely left-handed τ, respectively. The estimated number of the τ^- production with respect to the τ lepton energy, E_τ, is also plotted as a thin solid line. The results are calculated by using Eq. (29) with 100% particle detection efficiency for simplicity. For the above parameters, 113 events of τ^- are produced and 13 (20) of those decay into π^- (ℓ^-) mode.

The π^- and ℓ^- distributions have peak in the low energy region, and in this region the polarization dependence becomes large. As we pointed out in the previous section, the polarization dependence is opposite between π^- and ℓ^-, and is more significant in π^- than in ℓ^-. In the peak region, the polarization dependence affect the distribution around 30% (15%) for the π^- (ℓ^-) decay mode. Expected statistics is rather small in the current design of the CNGS experiments. However, the likelihood probability of each event will be affected significantly by the τ polarization effects. The characteristic feature of our prediction is that the produced τ^- is almost fully polarized and that it has non-zero transverse component of the spin vector, namely s_x of Eq. (7). The observed patterns of the π^- and ℓ^- energy distributions in the laboratory frame then follow from the energy angular distributions in the polarized τ rest frame[4].

Fig. 5 shows the azimuthal angle distribution of π^- (thick lines) and ℓ^- (thin lines). The azimuthal angle $\varphi_{\mathrm{i}=\pi,\ell}$ is given by $d\Omega_{\mathrm{i}} = d\cos\theta_{\mathrm{i}}\, d\varphi_{\mathrm{i}}$ in Eq. (29), and is measured from the scattering plane where $\varphi_{\mathrm{i}} = \pi/2$ is along the $\vec{p}_\nu \times \vec{p}_\tau$ direction in the laboratory frame, in which the z-axis is taken along the direction of the τ momentum. Solid lines show the distributions from τ^- with the predicted τ polarization, and dashed lines show those from unpolarized τ. The results of purely left-handed τ are the same as those for the

[4]We may note that we checked all our results by using TAUOLA (the Monte Carlo program to simulate decays of τ leptons) [25].

unpolarized τ. Since both unpolarized and purely left-handed τ^- have zero component of perpendicular polarization, they give flat azimuthal distributions. The azimuthal angle distributions can be measured by tracking the trajectory of τ leptons by emulsion detectors in the OPERA experiment, or by reconstructing the hadronic cascades from neutrino-nucleon scattering. As is the case of energy distribution, π^- and ℓ^- decay mode show the opposite feature and polarization dependence is clearer on π^- mode than ℓ^- mode. At $\varphi = 0$ or $|\pi|$, the dependence of the τ polarization affects the distribution by about 47% (16%) for the π^- (ℓ^-) decay. Even though the number of event is limited, it may be possible to obtain a hint of such large asymmetries.

Finally we comment on the contributions of the neutrino oscillation parameters to our results. The number of τ^- production is very sensitive to the value of δm^2_{13}. When we take Eq. (26) but $\delta m^2_{13} = 3 \times 10^{-3}$ eV^2, about 50 more events of τ^- are obtained. On the other hand, the produced τ^- decreases (about 10% maximum) for the larger (smaller) value of $\sin^2 2\theta_{13}$ ($\sin^2 2\theta_{23}$). However those parameters do not change much the impacts of the τ^- polarization on the energy and angular distributions of the τ decay products.

4 Conclusion

In this article, we have studied the effects of the spin polarization of τ^- produced in neutrino-nucleon scattering on the subsequent decay distributions. The calculation of the cross section and the spin polarization of τ^- production processes, QE, RES and DIS, were reviewed and the decay distributions of τ^- into π^- or $\ell^-(= e^-, \mu^-)$ modes were considered. Taking into account the polarization of produced τ^-, we calculated the energy and azimuthal angle distributions of π^- and ℓ^- in the laboratory frame, for the experimental setup of the CNGS long baseline project, OPERA and ICARUS experiments.

We found that the decay particle distributions in the laboratory frame are significantly affected by the τ^- polarization. Rather strong azimuthal asymmetry of π^- and ℓ^- about the τ momentum axis is predicted, which may have observable consequences even at small statistics experiments.

Before closing, let us mention about the decay particle distribution from τ^+, although there is no plan to use $\bar{\nu}_\mu$ beam in the CNGS experiments so far. In this case the strong azimuthal asymmetry predicted for the τ^- decay is not expected because the transverse component of the τ^+ polarization is rather small, as shown in Fig. 12 of Ref. [6].

Acknowledgments

K.M. would like to thank T. Morii for encouragements and S. Aoki for valuable comments. H.Y. would like to thank J. Kodaira for encouragement and RIKEN BNL Research Center for helpful hospitality during his stay. The work of K.H. is partially supported by the core university exchange program of JSPS.

References

[1] Z. Maki, M. Nakagawa, and S. Sakata, Prog. Theor. Phys. 28 (1962) 870.

[2] CNGS project home page, http://proj-cngs.web.cern.ch/.

[3] e.g. A. Rubbia, Nucl. Phys. B (Proc. Suppl.) 91 (2001) 223,
see also ICARUS Collaboration home page, http://pcnometh4.cern.ch/.

[4] OPERA Collaboration home page, http://operaweb.web.cern.ch/.

[5] See e.g., V. Barger et al., Phys. Rev. D 65 (2002) 053016; P. Huber et al., Phys. Rev. D 70 (2004) 073014.

[6] K. Hagiwara, K. Mawatari, and H. Yokoya, Nucl. Phys. B 668 (2003) 364; Erratum-ibid. 701 (2004) 405.

[7] K.S. Kuzmin, V.V. Lyubushkin, V.A. Naumov, Mod. Phys. Lett. A 19 (2004) 2815; K.S. Kuzmin, Seminar a KEK on Feb. 15, 2005.

[8] C.H. Llewellyn Smith, Phys. Rep. 3 (1972) 261.

[9] Particle Data Group (S. Eidelman et al.), Phys. Lett. B 592 (2004) 1.

[10] V. Bernard, L. Elouadrhiri, and U. Meissner, J. Phys. G 28 (2002) R1.

[11] K. Hagiwara, K. Mawatari, and H. Yokoya, Phys. Lett. B 591 (2004) 113.

[12] P.A. Schreiner and F. Von Hippel, Nucl. Phys. B 58 (1973) 333.

[13] S.K. Singh, M.J. Vicente Vacas, and E. Oset, Phys. Lett. B 416 (1998) 23.

[14] L. Alvarez-Ruso, S.K. Singh, and M.J. Vicente Vacas, Phys. Rev. C 57 (1998) 2693; and references therein.

[15] E.A. Paschos, J.Y. Yu, and M. Sakuda, Phys. Rev. D 69 (2004) 014013.

[16] M.G. Olsson, E.T. Osypowski, and E.H. Monsay, Phys. Rev. D 17 (1978) 2938.

[17] A.D. Martin et al., Eur. Phys. J. C 23 (2002) 73.

[18] The CHOOZ Collaboration (M. Apollonio et al.), Eur. Phys. J. C 27 (2003) 331.

[19] The Palo Verde Collaboration (F. Boehm et al.), Phys. Rev. D 64 (2001) 112001.

[20] B. Kayser, in Review of Particle Physics, Phys. Lett. B 592 (2004) 1, pp. 145–153, and references therein.

[21] The KamLAND Collaboration (T. Araki et al.), Phys. Rev. Lett. 94 (2005) 081801.

[22] The Super-Kamiokande Collaboration (Y. Ashie et al.), Phys. Rev. Lett. 93 (2004) 101801.

[23] The K2K collaboration (M.H. Ahn et al.), Phys. Rev. Lett. 90 (2003) 041801.

[24] M. Aoki et al., Phys. Rev. D 67 (2003) 093004; K. Hagiwara, Nucl. Phys. B (Proc. Suppl.) 137 (2004) 84.

[25] S. Jadach, Z. Was, R. Decker, and J H. Kuhn, Comput. Phys. Commun. 76 (1993) 361.